Interactions between internal tides and turbidity currents: an under-recognized process in deep-marine stratigraphy?

Euan L. Soutter[1], Ian A. Kane[1*], James E. Hunt[2], Veerle A. I. Huvenne[2], Miros S.J. Charidemou[2], Rebecca Garnett[2], Michael Edwards[2], Brian J. Bett[2], Furu Mienis[3], Rob A. Hall[4], Andrew R. Gates[2], Morgan Wolfe[2], Michael A. Clare[2]

[1]*Department of Earth and Environmental Science, University of Manchester, Manchester, M13 9PL, United Kingdom*

[2]*National Oceanography Centre, European Way, Southampton, SO14 3ZH, United Kingdom*

[3]*Department of Ocean Systems, Royal Netherlands Institute for Sea Research (NIOZ-Texel), Den Burg, the Netherlands*

[4]*Centre for Ocean and Atmospheric Sciences, School of Environmental Sciences, University of East Anglia, Norwich Research Park, Norwich, NR4 7TJ, United Kingdom*

[*]*Corresponding Author*

ABSTRACT

Deep-sea currents transfer sediment, nutrients, and pollutants, which drive climatic, ecological and geomorphological variation in the global ocean. The complex interaction of downslope currents and internal tides in submarine canyons has meant that interpreting their stratigraphic record and therefore reconstructing oceanic environments through geological time has proven challenging. We integrate flow measurements with sediment core observations from the Whittard Canyon, to determine whether the stratigraphic signature of turbidity current and internal tide interaction is preserved. Sand is transported by turbidity currents and re-worked by internal tides, forming a suite of characteristic deposits; near-bed flow measurements show that turbidity currents superposed on internal tides collectively exceed a critical bed shear stress for mobilizing fine sand at least 1% of a year, suspending sediment tens of meters above the bed over longer

periods. Using these observations, we present a framework to recognize this interaction in the stratigraphic record.

INTRODUCTION

The complex geomorphology of submarine canyons intensifies a variety of near-bed deep-sea flows (Inman et al. 1976; Shepard et al. 1979; Harris and Whiteway, 2011). Previous studies of modern submarine canyons worldwide suggest that the dominant processes driving intensified near-bed flows are typically internal tides and turbidity currents (Gardner, 1989; Maier et al. 2019; Pope et al. 2022). Internal tides are tidal-frequency gravity waves within a stratified water column that are generated by surface tidal flows across submarine slopes (e.g., Gardner, 1989). They become focused and amplified within the steep walls of submarine canyons (van Haren et al., 2022), thus influencing the transport and burial efficiency of organic carbon and pollutants (Maier et al. 2019). Turbidity currents are turbulent mixtures of water and particulates, typically terrigenous sediment, that flow downslope owing to their excess density; their deposits are a major component of the stratigraphic record (Mutti and Normark, 1987).

Stratigraphic studies have focused on deposits of turbidity currents (‘turbidites’) for decades; however, a mixture of bottom current processes likely affect the stratigraphic record of most systems to varying degrees (e.g. Rodrigues et al. 2022). Internal tides in particular have attracted significantly less attention, despite their capacity to resuspend and transport sediment in deep-sea environments worldwide (e.g. Shepard et al. 1974). This under-representation results from: i) a paucity of studies that link direct measurements of internal tides and turbidity currents with their deposits in the present day (e.g., Maier et al. 2019; Normandeau et al. 2023); and ii) an interpretative bias toward turbidity current processes in the ancient, making interpretations of internal tide influence in the deep-marine sedimentary record rare or equivocal (e.g., Zhenzhong and Eriksson, 1991; Shanmugam, 2003; 2021; He et al. 2008; Dykstra, 201; Pomar et al. 2012).

Direct flow monitoring close to coring sites is required to verify these interpretations and enable the robust identification of internal tide influence in the stratigraphic record.

Our study area is the Whittard Canyon (WC), located 300 km from land on the NE Atlantic margin (Amaro et al. 2016). Our first aim is to determine the relative importance of different current types on the sediment transport regime within the WC, with the hypothesis being that internal tides and turbidity currents are the dominant near-bed currents moving sediment along the canyon (Hall et al. 2017; Heijnen et al. 2022), and that the effect of these currents can be differentiated in the canyon stratigraphy. We assess this aims by integrating sedimentological observations, derived from sediment cores, with one year of monitoring of near-bed currents in the WC.

METHODS

Our study focuses on the Eastern Branch of the WC, and extends recent work that revealed both energetic internal tides and sub-annual turbidity currents (Fig. 1; Heijnen et al., 2022). Currents were measured for more than a year (June 2019 to August 2020) using a downward-looking 600 kHz acoustic Doppler current profiler (ADCP) located 30 m above the canyon thalweg on a mooring deployed on the 1591 m isobath (Fig. 1). The ADCP measured a vertical profile of current velocity and echo intensity between the instrument and seabed every 5 minutes with a vertical resolution of 1 m. Horizontal velocity was analyzed in a reference frame orientated along-canyon (30° clockwise from north) (Fig. 1E, F), and echo intensities provide a proxy for the amount of suspended sediment (Haalboom et al. 2021). The ADCP velocities and sedimentological data, derived from cored sections, were used to calculate whether shear stresses exerted on the bed were sufficient to move or suspend sediment (Niño et al., 2003; Garcia, 2008), thus allowing the sediment transport regime within the canyon to be assessed. Dimensionless

Shield's shear stresses were estimated from the maximum speed, the height of that speed (Fig. S4), and assuming a 1% sediment concentration in the current (Niño et al., 2003) for the median grain size (121 μm) sampled in the sediment trap of the mooring (Heijnen et al., 2020). Velocity is presented as the along-canyon velocity, where positive values refer to down-canyon flow, and negative values to up-canyon flow (Fig. 3A).

In order to test the link between current measurements and the stratigraphic record, we analyzed five piston-cores, which reached 1.0 to 5.5 m below seafloor (Fig. 2; 3; S1; S2; S7). While we cannot make an absolute tie between the flow monitoring and cored deposits, sediment accumulation rates of ~1.2 cm/yr (derived from ^{210}Pb dating of the nearest box-core to the cored sections; 10 km up-slope of core 75; Kranenburg et al. 2018), indicate the recovered core sections were deposited entirely during highstand conditions that were likely equivalent to those in the present day. This therefore supports the use of present-day hydrodynamic conditions as representative of those during deposition of the cored stratigraphy, in a similar manner to prior studies in other canyons (e.g. Symons et al., 2017). Core analysis included: 1) X-ray imaging, 2) micro-XRF scanning at 2 mm resolution (Rothwell et al., 2006); 3) magnetic susceptibility measurements at 5 mm resolution; and 4) visual sedimentological descriptions (Fig. 2; S7). The chemo-stratigraphy of the cored sections was analyzed using K-means clustering of the XRF-data, to assess millimetre-scale geochemical trends that cannot be visually resolved (Fig. S2).

RESULTS

Throughout the ADCP deployment, the flow regime was dominated by semidiurnal up- and down-canyon currents (Fig. 4D; S3), modulated from ± ~0.6 m/s to ± ~0.3 m/s by the spring-neap tidal cycle. These currents were capable of transporting, but more rarely suspending, fine sand (Fig. 4). These oscillating currents were punctuated by six asynchronous, shorter duration (several

hours) and higher velocity (up to 5.8 m/s) down-canyon currents that consistently attained shear stresses capable of suspending fine sand (Fig. 4; S3).

The sandiest core samples (75 & 74), ~20 km down-canyon of the mooring, are composed of mud and silty-mud punctuated by 1-12 cm thick, structureless fine-grained sand beds, with sharp or erosive bases and sharp or rippled bed tops (Fig. 2). Sharp tops feature abrupt grading, from fine sand upwards to mud, and ripples are often draped with mud. Inverse-to-normal grading occurs in some sand beds, where grading from silt to sand to silt corresponds to increasing then decreasing Si contents (Fig. 2). Such beds often occur in bundles of multiple sand-mud 'couplets' (Fig. 2).

Thinner (< 1 cm) silt and fine sand laminae and laminasets are interspersed throughout these sandy cores, occurring much more frequently than thicker beds (Fig. 2), and often forming starved ripples (Fig. 2). The fine scale and high frequency of these deposits is reflected in the XRF-derived clusters, as mm-scale interbeds of low-Si, high-Ca and high-Ti muds and higher-Si, lower-Ca, lower-Ti sands. Magnetic susceptibility is higher within the lower-Si, muddier intervals, compared to sandier intervals (Fig. S5). The thicker sand beds and thinner sand and silt lamina share the same geochemical signature.

DISCUSSION

The semidiurnal current velocities measured in the Whittard Canyon have been observed elsewhere in the Canyon (e.g., Hall et al., 2017), and many other submarine canyons (e.g., Maier et al., 2019; Fig. S6), and are interpreted to relate to internal tides. The higher velocity oscillations seen twice per month are coincident with surface spring tides, while lower velocity oscillations coincide with neap tides (Fig. 4), albeit with a sub-daily phase lag between the surface and internal tides (Heijnen et al. 2022). The higher velocity and episodic down-canyon velocity

measurements in the Canyon are interpreted as turbidity currents that initiated near the canyon head (Heijnen et al., 2022). Similar turbidity currents have been observed in many other submarine canyons, episodically overprinting background hydrodynamic conditions (e.g., Azpiroz-Zabala et al., 2018).

The presence of sharp or erosively-based fine sand beds within cores 74 and 75 (structureless or normally-graded) are indicative of deposition from the waning turbidity currents measured here (Fig. 3), forming a turbidite. Some depositional features of these beds are inconsistent with 'simple' deposition from waning turbidity currents, however, and indicate the influence of an additional process. Mounded bed tops and starved ripples indicate re-working of sediment on the seafloor by dilute or clear-water currents (Shanmugam et al., 1993). Similarly, sharp-topped beds and inverse-to-normally graded beds suggest more complicated shear stress variations on the canyon floor, such as by internal tides.

The sharp tops of many turbidites can be explained by the action of these internal tides, with the fine-grained tail of the turbidity currents being either: 1) prevented from settling by internal tides; or 2) winnowed by internal tides after deposition. Re-working of the entire bed, instead of the top alone, may be recorded as inverse-to-normally graded beds, with the turbiditic sand completely re-worked and re-deposited over a waxing and waning tidal cycle (Fig. 2; Pomar et al. 2012; Shanmugam et al., 2021). A similar process can be invoked for mud-draped ripples, where ripples form as the internal tidal velocity waxes, and mud is deposited as it wanes (Fig. 3) (Dykstra, 2011). The mm-scale, sand laminasets and starved ripples, that pervade the proximal cored sections, may be recycled remnants of such a process, where the consistent action of internal tides moves and deposits sediment continuously across the canyon floor after being deposited within the canyon by turbidity currents (Fig. 2; 3). Tidally-forced transport and deposition may also

explain the tendency for these deposits to stack into bundles of similar thicknesses (Fig. 2), with bundles of thick sand-mud pairs formed during periods of higher near-bed current velocities from energetic internal tides during springs, as observed in tidally-influenced shallow-marine environments (Visser, 1980). These bundles are not preserved throughout the stratigraphy, which may be due to periodic turbidity currents of variable magnitudes obscuring any consistent tidal signature, and sand availability on the seabed being limited by turbidity current occurrence and hemipelagic deposition, preventing a continuous record of tidal action.

These sedimentary structures may also form purely via turbidity current processes, such as through deflection and oscillation of turbidity currents interacting with seafloor topography (Tinterri et al., 2016), velocity pulsing within individual turbidity currents (Cunningham and Arnott, 2021), and flow rheology transitions (Baker and Baas, 2020). However, we argue that internal tides are a more likely origin for these deposits, due to: 1) the direct nearby measurements of internal tides with magnitudes capable of transporting and depositing these sediments; 2) the lack of pulsing or reflection observed in these turbidity currents, 3) the frequency and co-occurrence of a variety of different depositional features related to tides, such as mud-draped ripples; and 4) the similarity of these sediments to others linked to internal tides (e.g. Maier et al., 2019; Shanmugam et al., 2021; Normandeau et al. 2023).

IMPLICATIONS AND CONCLUSIONS

Our results show how flow interactions can modify stratigraphic records, which has wide-reaching implications. Prior studies have used sedimentary structures within turbidites to reconstruct past natural hazards, wherein rhythmic mud-sand bundles have been attributed to earthquakes and their aftershocks, or pulses in river floods (Mulder et al., 2003; Wils et al., 2021). However, spring-neap variations in bed shear stress are equally capable of creating such a stacked

depositional signature, implying caution in interpretation where direct constraint in hydrodynamic conditions is absent. Turbidity currents can be highly efficient agents of organic carbon and pollutant transport and burial within submarine canyons (Masson et al., 2010; Zhong et al., 2021). However, recurrent reworking of turbidites by internal tides may dramatically reduce the efficiency of that burial; exhuming fine-grained sediments that typically comprise the most organic-rich components (Masson et al., 2010) and redistributing previously-sequestered pollutants such as microplastics (Pohl et al., 2020). Our new results contribute to a growing recognition that 'mixed' sedimentary systems, where multiple processes interact (rather than operate in isolation), are the rule in the deep sea rather than the exception (e.g., Rodrigues et al., 2022).

ACKNOWLEDGMENTS

We thank the British Ocean Sediment Core Research Facility (BOSCORF) for supporting the generation of XRF core scanning / X-radiography / MSCL data used in this study. We also thank the Chief Scientist and Science Party, and the Captain and crew of RRS *James Cook* cruise 36 for collecting the sediment cores, and the Chief Scientist, Science Party, Captain and crew of RRS *Discovery* cruises DY103 and DY116 for deploying and collecting the mooring. These cruises and a fellowship held by ES were funded by the Climate Linked Atlantic Sector Science (CLASS) programme (grant number NE/R015953/1) and its predecessors OCEANS2025 and MAREMAP, supported by UK Natural Environment Research Council National Capability funding. FM was supported by the Innovational Research Incentives Scheme of the Netherlands Organisation for Scientific Research (NWO-VIDI grant no. 0.16.161.360).

DATA AVAILABILITY STATEMENT

The current monitoring data recorded from the 600 kHz ADCP on the M1 mooring are available via the British Oceanographic Data Centre at: https://www.bodc.ac.uk/resources/inventories/cruise_inventory/report/17695/. Further information and data pertaining to the mooring design are available in the NERC cruise report (http://nora.nerc.ac.uk/id/eprint/525366). Current monitoring data from the 75 kHz ADCP on the M2 mooring are available via the NIOZ Data Archive System at https://dataverse.nioz.nl/dataset.xhtml?persistentId=doi:10.25850/nioz/7b.b.7c. Bathymetric data for the Whittard Canyon are available from the EMODnet bathymetry portal at https://portal.emodnet-bathymetry.eu/. Meterological monitoring data from the K1 (https://www.metoffice.gov.uk/weather/specialist-forecasts/coast-and-sea/observations/162029) and Brittany buoy (https://www.metoffice.gov.uk/weather/specialist-forecasts/coast-and-sea/observations/162163) can be requested under open access for research purposes from MetOffice DataPoint (https://www.metoffice.gov.uk/services/data/datapoint). Cores are housed at the BOSCORF facility (https://boscorf.org/core-repository/collections) and are available to view upon request. Data analysed in this study are presented in S1-S9 of the supplementary material.

FIGURE CAPTIONS

Figure 1. Location of data used in this study. A) Location of the land-detached Whittard Canyon on the NE Atlantic (Celtic) margin. B) Location of the mooring and cored sections analyzed along the Eastern branch of the Whittard Canyon. C) Longitudinal profile and depth of the mooring and cored sections along the Canyon (profile on B). D) Cross-sections through each mooring and cored section (section locations on B). Contour intervals are 100 m. E, F) Example ADCP velocity measurements from M1, showing internal tides (E, F) and turbidity currents (F).

Figure 2: Sedimentary facies and x-ray-derived laminographs typical of sand-rich cored sections within the Canyon (example from core 74). All core images in Fig. S7. The sedimentary facies,

such as mud-draped ripples and rhythmic bundles, are indicative of turbidity current and internal tide interaction. Core disturbance causes some bed convexity.

Figure 3: Data from acoustic Doppler profiler at mooring M1 (location on Fig. 1). A. Maximum along-canyon velocity per 5-minute interval over the measured period. Negative values refer to up-canyon flow, while positive values are down-canyon flow. Note the constant background of semidiurnal tides punctuated by faster, shorter duration turbidity currents. Black arrows denote suspension of fine sand, grey arrows denote motion (traction) of fine sand based on Shield's mobility criteria (D; E). B. Expanded series of internal tide velocities. Note the increased velocity magnitude at spring tides, which results in more frequent suspension of fine sand from the canyon floor. C. Expanded series of echo intensities. Echo intensity increases during spring tides, indicating greater suspended sediment in the water column. D, E. Up-canyon (D) versus down-canyon (E) directed currents plotted on Shield's mobility diagram for fine sand (f.s.) and silt (si.). Down-canyon flows are more frequently able to form a turbulent, or 'rough', boundary layer and suspend fine sand than up-canyon flows. Initiation of motion and suspension curves from Niño et al. (2003) and Garcia et al. (2008). Boundary layers from Garcia et al. (2008). F. Shields parameter distribution. Motion of sediment is rare (~1 % of time) for fine sand.

Figure 4. Synthesis of the stratigraphy expected in deep-marine systems dominated by down-slope turbidity currents (A) and deep-marine systems influenced by both downslope turbidity currents and internal tides (B). Other sedimentary features identified in this study, such as inverse-to-normal grading, would also be expected in internal-tide influenced successions (B).

REFERENCES CITED

Amaro, T., Huvenne, V.A.I., Allcock, A.L., Aslam, T., Davies, J.S., Danovaro, R., De Stigter, H.C., Duineveld, G.C.A., Gambi, C., Gooday, A.J. and Gunton, L.M., 2016. The Whittard

Canyon–A case study of submarine canyon processes: Progress in Oceanography, v. 146, p. 38-57.

Azpiroz-Zabala, M., Cartigny, M.J., Talling, P.J., Parsons, D.R., Sumner, E.J., Clare, M.A., Simmons, S.M., Cooper, C. and Pope, E.L., 2017, Newly recognized turbidity current structure can explain prolonged flushing of submarine canyons: Science advances, v. 3, p.e1700200.

Baker, M.L. and Baas, J.H., 2020, Mixed sand–mud bedforms produced by transient turbulent flows in the fringe of submarine fans: Indicators of flow transformation: Sedimentology, v. 67, p. 2645-2671.

Dykstra, M., 2012., Deep-water tidal sedimentology: In: Davis Jr., R.A., Dalrymple, R.W. (Eds.), Principles of Tidal Sedimentology, pp. 371–395.

Garcia, M., 2008, Sedimentation Engineering: Processes, Measurements, Modeling and Practise: American Society of Civil Engineers.

Gardner, W.D., 1989, Periodic resuspension in Baltimore Canyon by focusing of internal waves: Journal of Geophysical Research: Oceans:, v. 94, p. 18185-18194.

Haalboom, S., H. de Stigter, G. Duineveld, H. van Haren, G.-J. Reichart and F. Mienis. 2021. Suspended particulate matter in a submarine canyon (Whittard Canyon, Bay of Biscay, NE Atlantic Ocean): Assessment of commonly used instruments to record turbidity: Marine Geology, 106439.

Hall, R.A., Aslam, T. and Huvenne, V.A., 2017, Partly standing internal tides in a dendritic submarine canyon observed by an ocean glider: Deep Sea Research Part I: Oceanographic Research Papers, v. 126, p. 73-84.

Harris, P.T. and Whiteway, T., 2011, Global distribution of large submarine canyons: Geomorphic differences between active and passive continental margins: Marine Geology, v. 285, p. 69-86.

He, Y., Gao, Z., Luo, J., Luo, S. and Liu, X., 2008, Characteristics of internal-wave and internal-tide deposits and their hydrocarbon potential: Petroleum Science, v. 5, p. 37-44.

Heijnen, M.S., Mienis, F., Gates, A.R. et al., 2022, Challenging the highstand-dormant paradigm for land-detached submarine canyons: Nature Communications, v. 13, p. 3448.

Inman, D.L., Nordstrom, C.E. and Flick, R.E., 1976. Currents in submarine canyons: An air-sea-land interaction: Annual Review of Fluid Mechanics, v. 8, p. 275-310.

Kranenburg, J., Mienis, F., J.H.J.L. van der Lubbe, J.H.J.L., 2018., The Unknown Role of Whittard Canyon: Pathway or Sink for Organic Carbon: MSc Thesis, Royal Netherlands Institute for Sea Research, 73 p.

Maier, K.L., Rosenberger, K.J., Paull, C.K., Gwiazda, R., Gales, J., Lorenson, T., Barry, J.P., Talling, P.J., McGann, M., Xu, J. and Lundsten, E., 2019. Sediment and organic carbon

transport and deposition driven by internal tides along Monterey Canyon, offshore California: Deep Sea Research Part I: Oceanographic Research Papers, 153, p.103108.

Masson, D.G., Huvenne, V.A.I., De Stigter, H.C., Wolff, G.A., Kiriakoulakis, K., Arzola, R.G. and Blackbird, S., 2010, Efficient burial of carbon in a submarine canyon: Geology, v. 38, p. 831-834.

Mulder, T., Syvitski, J.P., Migeon, S., Faugères, J.C. and Savoye, B., 2003. Marine hyperpycnal flows: initiation, behavior and related deposits. A review: Marine and Petroleum Geology, v. 20, p. 861-882.

Mutti, E. and Normark, W.R., 1987. Comparing examples of modern and ancient turbidite systems: problems and concepts, in: *Marine Clastic Sedimentology*, Springer, Dordrecht. p. 1-38.

Niño, Y., Lopez, F. and Garcia, M., 2003. Threshold for particle entrainment into suspension: Sedimentology, v. 50, p. 247-263.

Normandeau, A., Dafoe, L.T., Li, M.Z., Campbell, D.C. and Jenner, K.A., 2024. Sedimentary record of bottom currents and internal tides in a modern highstand submarine canyon head: Sedimentology. In press.

Pohl, F., Eggenhuisen, J.T., Kane, I.A. and Clare, M.A., 2020. Transport and burial of microplastics in deep-marine sediments by turbidity currents: Environmental Science & Technology, v. *54*(7), p. 4180-4189.

Pomar, L., Morsilli, M., Hallock, P. and Bádenas, B., 2012, Internal waves, an under-explored source of turbulence events in the sedimentary record: Earth-Science Reviews, v. 111, p. 56-81.

Pope, E.L., Cartigny, M.J., Clare, M.A., Talling, P.J., Lintern, D.G., Vellinga, A., Hage, S., Açikalin, S., Bailey, L., Chapplow, N. and Chen, Y., 2022. First source-to-sink monitoring shows dense head controls sediment flux and runout in turbidity currents: Science Advances, v. 8, p.eabj3220.

Rodrigues, S., Hernández-Molina, F.J., Fonnesu, M., Miramontes, E., Rebesco, M. and Campbell, D.C., 2022, A new classification system for mixed (turbidite-contourite) depositional systems: Examples, conceptual models and diagnostic criteria for modern and ancient records: Earth-Science Reviews, p.104030.

Rothwell, R.G., Hoogakker, B., Thomson, J., Croudace, I.W. and Frenz, M., 2006, Turbidite emplacement on the southern Balearic Abyssal Plain (western Mediterranean Sea) during Marine Isotope Stages 1–3: an application of ITRAX XRF scanning of sediment cores to lithostratigraphic analysis: Geological Society, London, Special Publications, v. 267, p. 79-98.

342 Shanmugam, G., Spalding, T.D. and Rofheart, D.H., 1993, Traction structures in deep-marine,
343 bottom-current-reworked sands in the Pliocene and Pleistocene, Gulf of Mexico: Geology, v.
344 21, p. 929-932.

345

346 Shanmugam, G., 2003. Deep-marine tidal bottom currents and their reworked sands in
347 modern and ancient submarine canyons. Marine and Petroleum Geology, 20, pp.471-491.

348

349 Shanmugam, G., 2021. The turbidite-contourite-tidalite-baroclinite-hybridite problem:
350 orthodoxy vs. empirical evidence behind the "Bouma Sequence": Journal of
351 Palaeogeography, v. 10, p. 1-32.

352

353 Shepard, F.P., Marshall, N., McLoughlin, P.A., & Sullivan, G. G., 1979, Currents in
354 submarine canyons and other sea valleys: American Association of Petroleum Geologists,
355 Studies in Geology, no. 8.

356

357 Tinterri, R., Magalhaes, P.M., Tagliaferri, A. and Cunha, R.S., 2016, Convolute laminations
358 and load structures in turbidites as indicators of flow reflections and decelerations against
359 bounding slopes. Examples from the Marnoso-arenacea Formation (northern Italy) and Annot
360 Sandstones (south eastern France): Sedimentary Geology, v. 344, p. 382-407.

361

362 Wils, K., Deprez, M., Kissel, C., Vervoort, M., Van Daele, M., Daryono, M.R., Cnudde, V.,
363 Natawidjaja, D.H. and De Batist, M., 2021. Earthquake doublet revealed by multiple pulses in
364 lacustrine seismo-turbidites. *Geology*, *49*(11), pp.1301-1306.

365

van Haren, H., F. Mienis and G. Duineveld., 2022, Contrasting internal tide turbulence in a tributary of the Whittard Canyon: Continental Shelf Research, v. 236, 104679.

Visser, M, J., 1980, Neap-spring cycles reflected in Holocene sub-tidal large-scale bedform deposits: A preliminary note: Geology, v. 8, p. 543–546.

Xu, J.P., 2011, Measuring currents in submarine canyons: Technological and scientific progress in the past 30 years: Geosphere, v. 7, p. 868-876.

Zhenzhong, G. and Eriksson, K.A., 1991, Internal-tide deposits in an Ordovician submarine channel: Previously unrecognized facies?: Geology, v. 19, p. 734-737.

Zhong, G. and Peng, X., 2021. Transport and accumulation of plastic litter in submarine canyons—The role of gravity flows: Geology, v. 49, p. 581-586.

Figure 1.

A
200 km
ROI
UK
France
Celtic margin
Whittard Canyon
B
Spain
-6 [km] 0
latitude [°]
longitude [°]
B
Central Branch
Eastern Branch
10 km
M1
82
75
74
60
71
-4 [km] -0.1
C
seabed
depth [km]
down-canyon distance [km]
D
across-canyon distance [km]
E
up-canyon internal tide
down-canyon internal tide
height above seafloor [m]
time [hours]
F
down-canyon turbidity current
up-canyon internal tide
down-canyon internal tide
< -1 along-canyon velocity [ms⁻¹] > 1

Figure 2.

image
x-ray [lam]
Si/Ca
A
B
depth [m]
0.7
0.75
0.8
0.85
0.9
0.95
1.0
3.0
3.05
3.1
3.15
3.2
3.25
3.3
high-density sands
low-density muds
inverse-normal grading
sharp-based, high Si turbidite
erosion surface (?)
hummock-like bedform
bundle?
mud-draped ripples
inverse-normal grading
inverse-normal grading
low Si mud-drape
re-working of bed top
0.000
0.025
0.050
C
mounded-top
discontinuous laminae
discontinuous laminae
sharp-top
1 cm
D
re-worked bed top
bundle
erosive base
mounded bed top
1 cm
E
starved ripple
discontinuous laminae
1 cm

Figure 3.

max. velocity [all]

A

turbidity currents

expanded in B & C

suspension

motion

smoothed

down-canyon internal tides

turbidity currents

up-canyon internal tides

max. velocity [m/s]

time [days]

max. velocity [expanded]

B

spring tides

neap tides

smoothed

max. velocity [m/s]

time [days]

echo intensity [expanded]

C

more sediment in water column at spring tides

smoothed

echo intensity at max. velocity [count]

time [days]

down-canyon

up-canyon

Shields parameter distribution

D

E

F

smooth

t. rough

rough

si.

f.s.

init. susp

init. motion

τ_*

Re_p

proportion

~motion

~no motion

Figure 4.

A. Turbidity currents alone

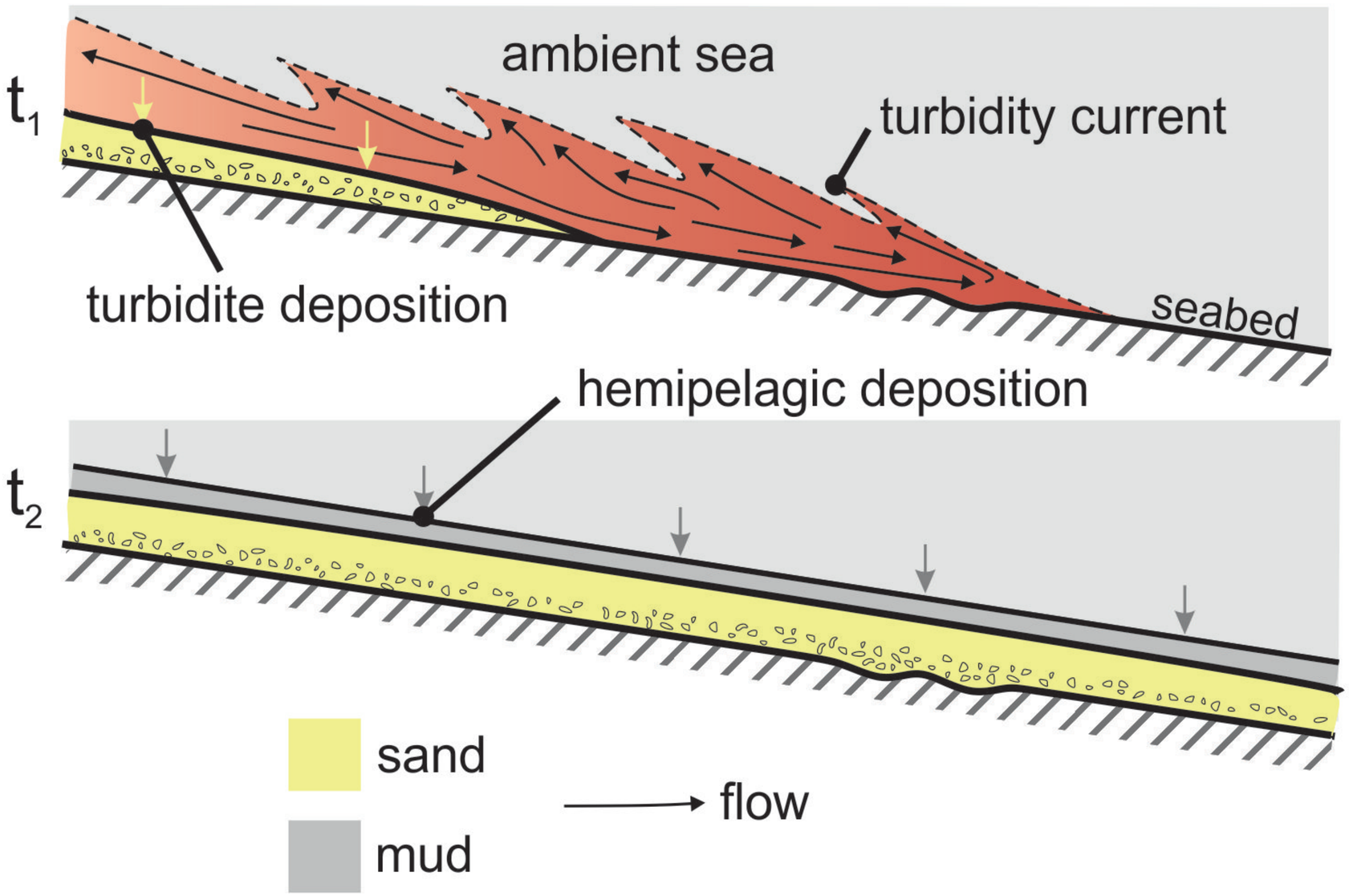

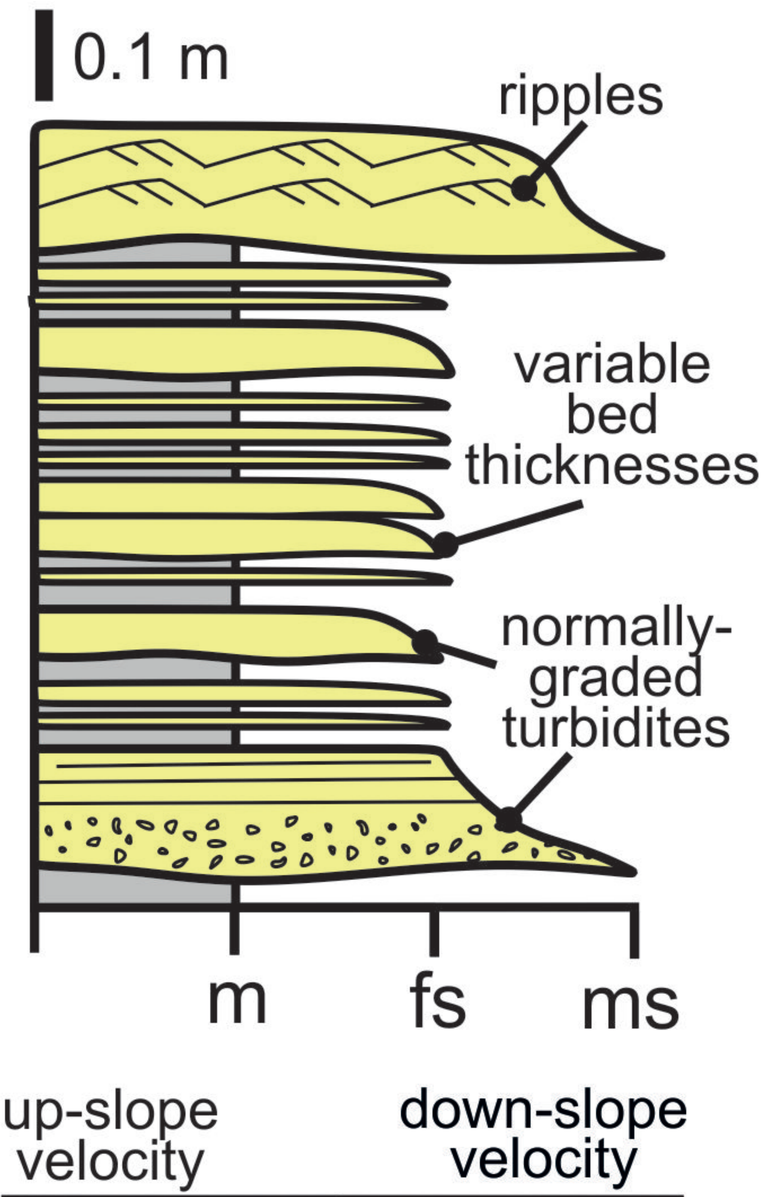

B. Turbidity currents with internal tides